

# RSC Advances



This is an *Accepted Manuscript*, which has been through the Royal Society of Chemistry peer review process and has been accepted for publication.

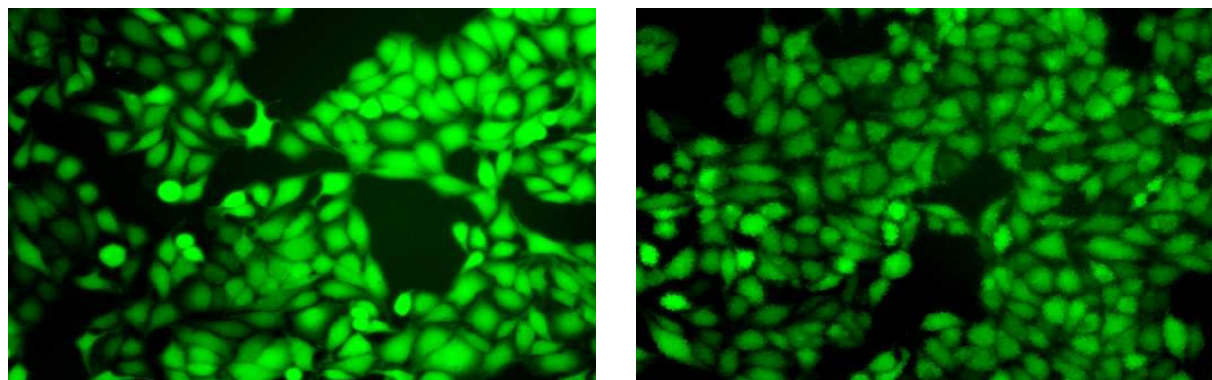
*Accepted Manuscripts* are published online shortly after acceptance, before technical editing, formatting and proof reading. Using this free service, authors can make their results available to the community, in citable form, before we publish the edited article. This *Accepted Manuscript* will be replaced by the edited, formatted and paginated article as soon as this is available.

You can find more information about *Accepted Manuscripts* in the [Information for Authors](#).

Please note that technical editing may introduce minor changes to the text and/or graphics, which may alter content. The journal's standard [Terms & Conditions](#) and the [Ethical guidelines](#) still apply. In no event shall the Royal Society of Chemistry be held responsible for any errors or omissions in this *Accepted Manuscript* or any consequences arising from the use of any information it contains.

**Graphical Abstract****Synthesis of chitosan-coated polyoxometalate nanoparticles against cancer and its metastasis**

Hamid Saeed Shah, Sachin A. Joshi, Ali Haider, Ulrich Kortz, Nisar-ur-Rehman, Jamshed Iqbal\*



HeLa cells, before and after treatment with nanoparticles

## Synthesis of chitosan-coated polyoxometalate nanoparticles against cancer and its metastasis

Hamid Saeed Shah<sup>[a]</sup>, Sachin A. Joshi<sup>[b,c]</sup>, Ali Haider<sup>[b]</sup>, Ulrich Kortz<sup>[b]</sup>, Nisar-ur-Rehman<sup>[a]</sup>  
and Jamshed Iqbal<sup>[a]\*</sup>

<sup>[a]</sup>Centre for Advanced Drug Research, Department of Pharmacy COMSATS Institute of Information Technology, Abbottabad, Postal Code 22060, Pakistan.

<sup>[b]</sup>Department of Life Sciences and Chemistry, Jacobs University, P.O. Box 750 561, 28725 Bremen, Germany.

<sup>[c]</sup>Dr. K. C. Patel Research and Development Centre, Charotar University of Science and Technology (CHARUSAT), Changa Dist., Anand 388421, India

### To whom Correspondence should address:

Prof. Dr. Jamshed Iqbal

Centre for Advanced Drug Research, Department of Pharmacy  
COMSATS Institute of Information Technology Abbottabad, Postal Code 22060, Pakistan

Telephone: +92-992-383591-96; Fax: +92-992-383441

E-mail: [drjamshed@ciit.net.pk](mailto:drjamshed@ciit.net.pk)

### Abstract

Three different Keggin-type polyoxometalates (POMs)  $[\text{PW}_{12}\text{O}_{40}]^{3-}$ ,  $[\text{TiW}_{11}\text{CoO}_{40}]^{7-}$ , and  $[\text{Ti}_2\text{PW}_{10}\text{O}_{40}]^{7-}$ , were synthesized and then encapsulated in chitosan to prepare nanoparticles, CS-PW<sub>12</sub>, CS-TiW<sub>11</sub>Co, and CS-Ti<sub>2</sub>PW<sub>10</sub>. The synthesized nanoparticles were physicochemically characterized in terms of particle size, zeta potential, entrapment efficiency and *in vitro* release of the entrapped POM. The most efficient formulation was CS-TiW<sub>11</sub>Co, with a particle size of  $105 \pm 6$  nm and an entrapment efficiency of  $87 \pm 12$  (%). The CS-TiW<sub>11</sub>Co nanoparticles showed the highest activity when tested against tissue nonspecific alkaline phosphatase (TNAP) with  $\text{IC}_{50} = 102.0 \pm 9.68$  nM. The anticancer

potential of the free POMs and their nanoparticles were also studied and CS-TiW<sub>11</sub>Co showed the highest inhibition ( $IC_{50} = 1.06 \pm 0.09$ ) on HeLa cells. To observe signs of apoptosis in HeLa cells, a DAPI staining was performed after treatment with CS-TiW<sub>11</sub>Co nanoparticles. Furthermore, the reactive oxygen species (ROS) production was examined by H<sub>2</sub>DCF-DA dye under a fluorescence microscope. Our study revealed that CS-TiW<sub>11</sub>Co nanoparticles are very effective in cancer treatment and its associated metastasis especially in osteoblastic lesion with minimal adverse effects on normal cells (Vero cells).

**Keywords:** Alkaline phosphatase, Cancer, Chitosan, Nanoparticles, Polyoxometalates.

### Introduction

Polyoxometalates (POMs) are discrete, anionic metal-oxides with potential applications in catalysis, material science, and medicine.<sup>1-5</sup> POMs are highly effective for the treatment of cancer, diabetes and infections associated with bacteria, viruses, and leishmania parasites.<sup>6</sup> POMs have excellent potential for the treatment of almost all types of cancers including pancreatic cancer<sup>7</sup>, leukemia<sup>8</sup>, hepatocellular carcinoma<sup>9</sup>, colon carcinoma<sup>10</sup>, ovarian cancer<sup>11</sup>, gastric cancer<sup>12</sup>. The exact mechanism of POMs causing cancer cell death is still unknown<sup>13</sup> but previous studies have shown that POMs have high potential to generate reactive oxygen species (ROS) which result into intracellular oxidative-stress causing hypoxia and cell death.<sup>14, 15</sup> Another mechanism to determine apoptosis is seen by the generation of DNA fragments of cancer cells when treated with different POMs.<sup>7, 10, 16, 17</sup>

Furthermore, cancers originating from kidney, prostate, breast and lungs have a tendency to metastasize into bones characterized by osteolytic and osteoblast formation.<sup>18</sup> Bisphosphonates are highly recommended to reduce pain associated with osteolytic bone metastasis<sup>19</sup>, whereas to the best of our knowledge no drug has been recommended to reduce osteoblastic lesion. The tissue non-specific alkaline phosphatase (TNAP) enzyme is involved in the hydrolysis of pyrophosphate (PPi) to form hydroxyapatite (HA) which triggers the process of mineralization (osteoblast activity).<sup>20</sup> POMs have shown an excellent potential to treat the abnormal functions of alkaline phosphatases commonly seen in hydroxyapatite deposition disease (HADD) that is associated with over-expression of alkaline phosphatase enzyme.<sup>21, 22</sup> In the light of the above mentioned role of TNAP it can be assumed that by blocking TNAP activity also osteoblast formation can be prevented during cancer metastasis.

There are two major reasons why POMs are not applied more frequently in medicine. Firstly, several POMs are not sufficiently stable at physiological pH, and secondly, due to the lack of selectivity they exhibit toxicity.<sup>14</sup> In order to render POMs more stable and less toxic to the surrounding non-cancerous cells, a surface modification is required, which may be accomplished by encapsulating POMs in a biodegradable polymer. Encapsulation of target molecules in biodegradable polymers ensures high protection of the drug in a physiological environment and allows for delivery of the drug at the target site.<sup>23-27</sup> The particle size is highly important for the determination of the fate of the nanoparticles. A 5-200 nm particle size range is highly efficient for targeting a specific organ because such particles can be effectively excreted from the kidneys and the reticuloendothelial system (RES) to reach the target site.<sup>28, 29</sup>

Chitosan is a polysaccharide composed of glucosamine and *N*-acetyl glucosamine linked by (1→4)  $\beta$ -glucosidic bonds obtained from chitin, which is widely present in the shells of crabs and the exoskeleton of shrimps.<sup>30</sup> Chitosan is very popular in the field of nanotechnology because of its inert nature, high availability, biocompatibility, low immunogenicity, and mucoadhesive nature.<sup>31</sup>

The objective of the present study was to evaluate the anticancer potential of three novel POMs enclosed in chitosan. These nanoparticles were prepared by ionotropic gelation technique and characterized by different physicochemical tools (FTIR, particle size, zeta potential, entrapment efficiency and dissolution studies). The entrapment efficiency and *in vitro* release of the POMs from the nanoparticles was also determined. The POMs were further tested against TNAP, whereas the anticancer activity was tested on HeLa cells. In addition, apoptosis and ROS production were observed with a fluorescence microscope.

## Results and discussion

### Preparation of chitosan/ POM nanocomplexes

The three Keggin-type POMs include phosphotungstates  $[\text{PW}_{12}\text{O}_{40}]^{3-}$ , Cobalt (Co) substituted Titanium (Ti) containing poly anion  $[\text{TiW}_{11}\text{CoO}_{40}]^{7-}$ , and Ti containing tungstates  $[\text{Ti}_2\text{PW}_{10}\text{O}_{40}]^{7-}$  were synthesized by following previously reported methods<sup>35-37</sup>. The selected POMs were highly stable at physiological pH (7.4). The nanoparticles were prepared by using the ionotropic gelation technique, in which the chitosan and the POM served as cation and anion, respectively.

### Characterization of the POMs and chitosan-POM nanoparticles

The POMs used here were characterized by FTIR and NMR ( $^{31}\text{P}$ ) spectroscopy (see Figures 2 and 3). It is evident from SEM analysis that the prepared chitosan-POM nanoparticles were slightly irregular in shape with particle size not more than  $<200$  nm (see Figure 4). The size distribution of the nanoparticles (Figure 5) was determined by dynamic light scattering (DLS). Electrophoretic light scattering was used to evaluate the stability and the surface charge of the nanoparticles. The particle diameter and the zeta potential of CS-PW<sub>12</sub> and CS-

Ti<sub>2</sub>PW<sub>10</sub> were determined as  $164 \pm 9$  nm and  $190 \pm 7$  nm, as well as  $+44.8 \pm 3.8$  mV and  $+47.4 \pm 6.1$  mV, respectively. The best formulation amongst the studied compounds was CS-TiW<sub>11</sub>Co, with a particle size diameter and zeta potential of  $105 \pm 6$  nm and  $+52.0 \pm 5.2$  mV, respectively (Table 1).

The overlaid FTIR spectra of CS, the three polyanions, and CS-POM nanoparticles are shown in Figure 3. The characteristic band of {PW<sub>12</sub>} at  $1633\text{ cm}^{-1}$  represents crystal waters, whereas for CS the spectral bands at  $1625\text{ cm}^{-1}$  and  $1081\text{ cm}^{-1}$  are due to N–H bending (amines) and C–O–C stretching, respectively.<sup>32,33</sup> The nanocomplex formed showed bands at  $1639\text{ cm}^{-1}$  and  $1087\text{ cm}^{-1}$  which indicate the presence of both chitosan and {PW<sub>12</sub>}. Similarly, the CS-TiW<sub>11</sub>Co nanocomplex showed bands at  $1614\text{ cm}^{-1}$  and  $1071\text{ cm}^{-1}$ , which are slightly different from the peaks in the chitosan and {TiW<sub>11</sub>Co} spectra (Figure 3). The confirmation of the nanocomplex CS-Ti<sub>2</sub>PW<sub>10</sub> was obtained when the  $1638\text{ cm}^{-1}$  and  $1085\text{ cm}^{-1}$  peaks appeared (Figure 3).

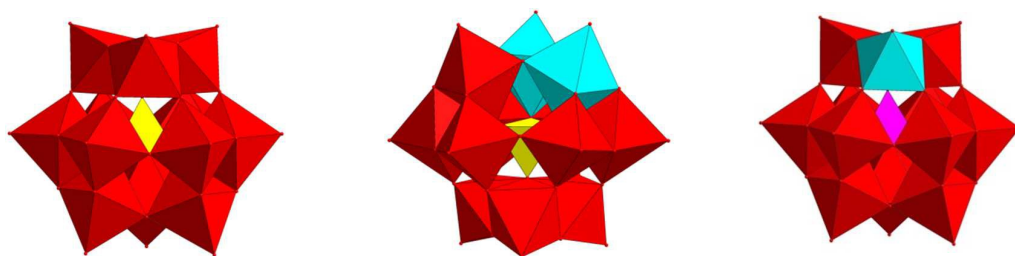


**Figure 1.** Polyhedral representation of polyanions  $[\text{PW}_{12}\text{O}_{40}]^{3-}$  (left),  $[\text{Ti}_2\text{PW}_{10}\text{O}_{40}]^{7-}$  (middle), and  $[\text{TiW}_{11}\text{CoO}_{40}]^{7-}$  (right). Yellow Phosphorous (P), Light green Titanium (Ti) and pink colour represents Cobalt (Co) element.

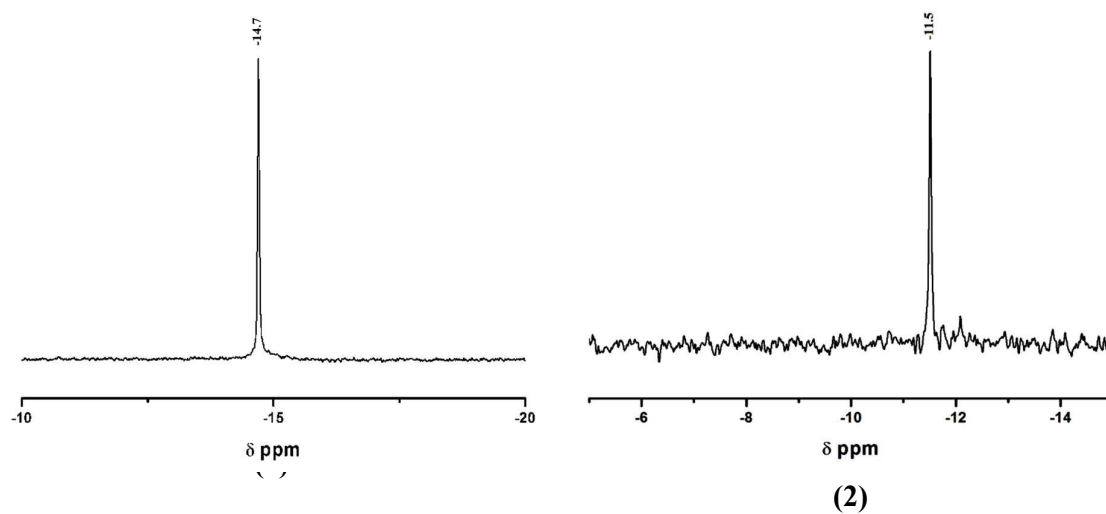


**Figure 2.**  $^{31}\text{P}$  NMR spectra of  $[\text{PW}_{12}\text{O}_{40}]^{3-}$  (left) and  $[\text{Ti}_2\text{PW}_{10}\text{O}_{40}]^{7-}$  (right) in  $\text{H}_2\text{O}/\text{D}_2\text{O}$

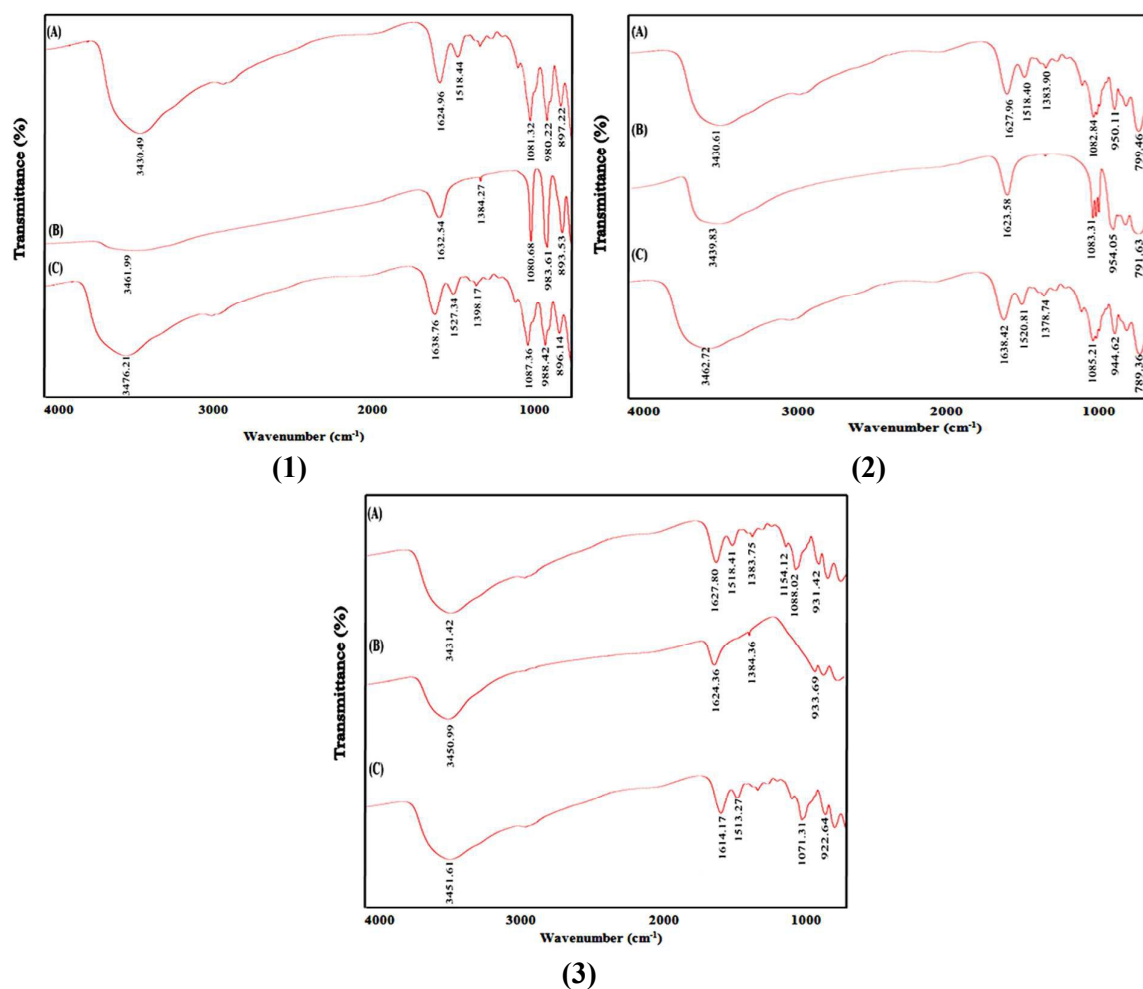


**Figure 3.** FTIR spectra of **1**: (a) Chitosan (CS) (b) {PW<sub>12</sub>} (c) CS-PW<sub>12</sub> nanoparticles; **2**: (a) Chitosan (CS) (b) {Ti<sub>2</sub>PW<sub>10</sub>} (c) CS-Ti<sub>2</sub>PW<sub>10</sub> nanoparticles; **3**: (a) Chitosan (CS) (b) {TiW<sub>11</sub>Co} (c) CS-TiW<sub>11</sub>Co nanoparticles

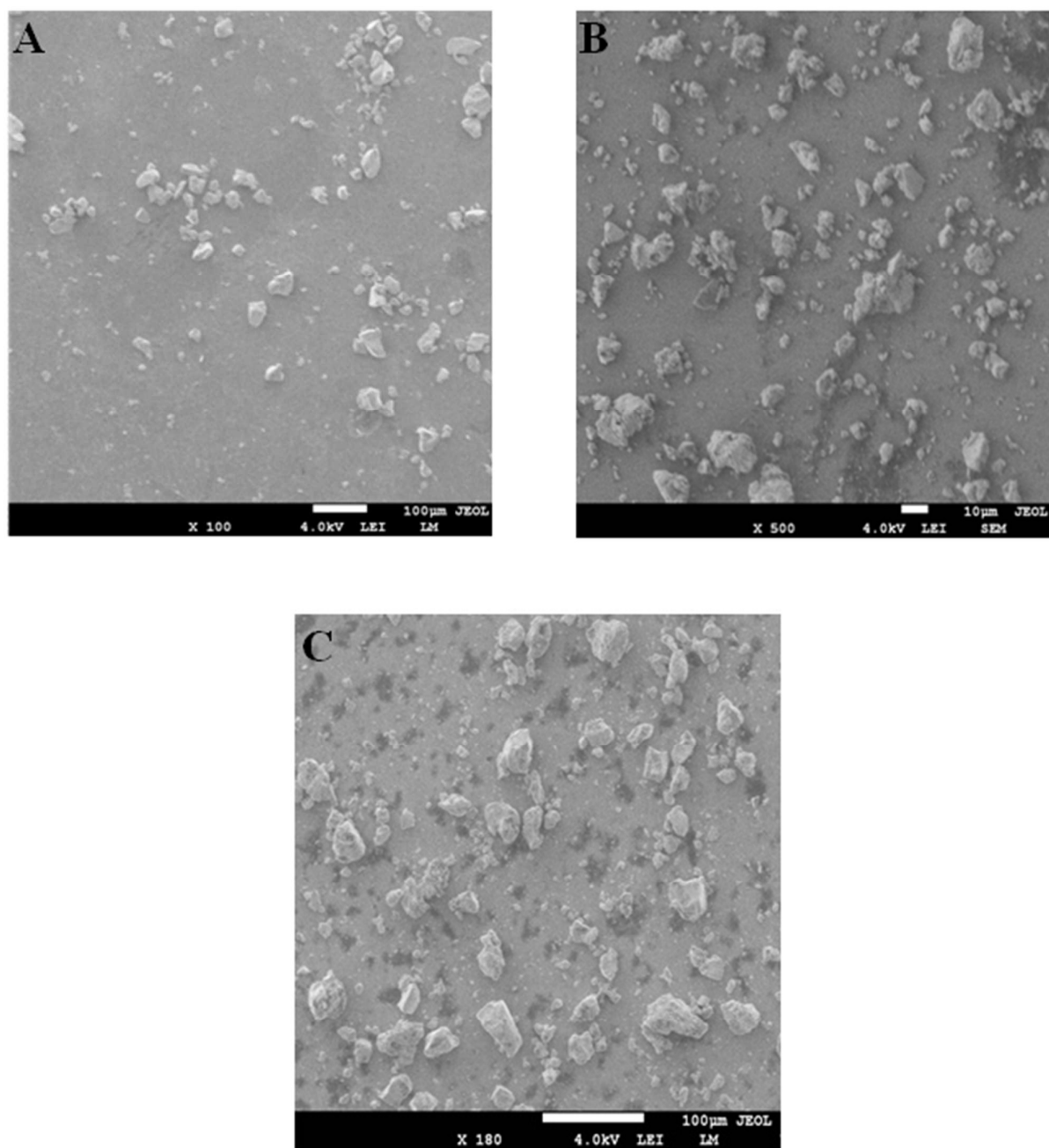


**Figure 4.** Surface morphology of nanoparticles CS-PW<sub>12</sub> (A), CS-Ti<sub>2</sub>PW<sub>10</sub> (B), and CS-TiW<sub>11</sub>Co (C).

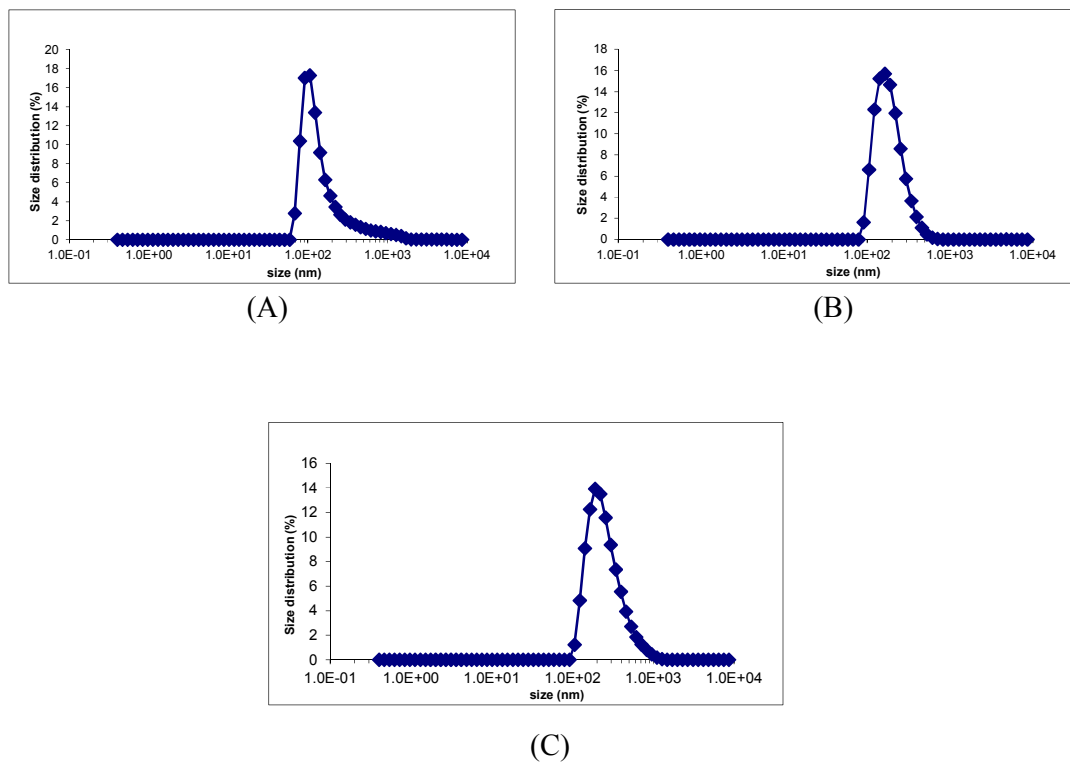


**Figure 5.** Size distribution of chitosan-POM nanoparticles, CS-TiW<sub>11</sub>Co (A); CS-PW<sub>12</sub> (B) and CS-Ti<sub>2</sub>PW<sub>10</sub> (C)

**Table 1.** Characterization of chitosan-POM nanoparticles

Code	Formula	CS/ POM ratio	Particle size ± SD (nm)	Zeta potential ± SD (mV)	Entrapment efficiency (%)
CS-TiW <sub>11</sub> Co	Chitosan-[TiW <sub>11</sub> CoO <sub>40</sub> ] <sup>7-</sup>	4:2	105 ± 6	+52.0 ± 5.2	87 ± 12
CS-PW <sub>12</sub>	Chitosan-[PW <sub>12</sub> O <sub>40</sub> ] <sup>3-</sup>	4:2	164 ± 9	+44.8 ± 3.8	83 ± 10
CS-Ti <sub>2</sub> PW <sub>10</sub>	Chitosan- [Ti <sub>2</sub> PW <sub>10</sub> O <sub>40</sub> ] <sup>7-</sup>	4:2	190 ± 7	+47.4 ± 6.1	91 ± 7

### Entrapment and release of drug from nanoparticles

The amount of drug entrapped in the chitosan-coated POM nanoparticles was determined spectrophotometrically. It was evident from the data that the entrapment efficiency (EE) of the selected nanoparticles was excellent and had a linear relationship with particle size (Table 1). The maximum EE was seen for CS-Ti<sub>2</sub>PW<sub>10</sub> (91 ± 7 %), while CS-TiW<sub>11</sub>Co and CS-PW<sub>12</sub> also had good percentages of drug entrapping, 87 ± 12 (%) and 83 ± 10 (%), respectively.

In order to understand the mechanism of POM release from the nanoparticles, *in vitro* dissolution studies were carried out for 96 h in PBS (pH 7.4) supplemented with lysozyme. The lysozyme was used to degrade the chitosan backbone by cleavage of the glycosidic bonds. When the release kinetics was studied and it became evident that the selected chitosan-POM nanoparticles followed concentration-dependent first order release kinetics with excellent regression coefficients R<sup>2</sup> (see Table 2). Similarly, the mechanism of POM release from chitosan was determined by using the Higuchi and Peppas models. The release of the POMs from chitosan was governed by a diffusion mechanism. The Peppas model confirmed that the release mechanism starts with erosion of the polymer matrix followed by diffusion ( $n > 0.45$ ) (Table 2).

**Table 2.** Release mechanism of POMs from CS in dissolution experiments

Code	Zero order (R <sup>2</sup> )	First order (R <sup>2</sup> )	Higuchi model (R <sup>2</sup> )	Peppas model (R <sup>2</sup> )	N
CS-PW <sub>12</sub>	0.748	0.999	0.998	0.997	0.607
CS-TiW <sub>11</sub> Co	0.710	0.996	0.995	0.991	0.568
CS-Ti <sub>2</sub> PW <sub>10</sub>	0.789	0.998	0.996	0.995	0.582

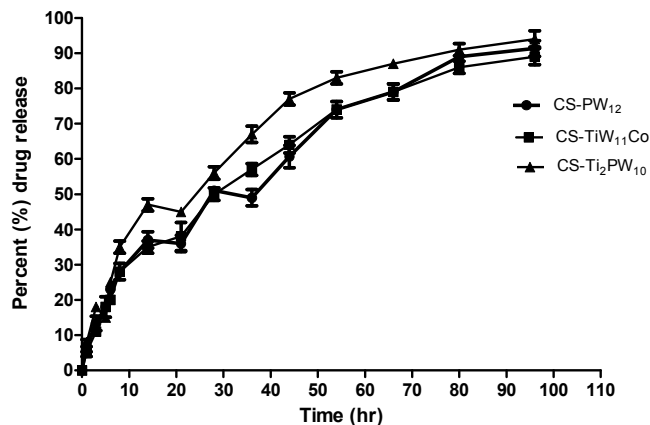


**Figure 6.** Dissolution profile of CS-POM nanoparticles at physiological pH 7.4

### Alkaline phosphatase inhibition studies

An inhibitor of tissue non-specific alkaline phosphatase (TNAP) enzyme may become a future drug for the treatment of malignant tumors, which mainly target bones. The activities of unbound POMs and chitosan-coated POMs against TNAP were studied and showed excellent  $IC_{50}$  values in the nanomolar range. The results obtained from the colorimetric assay confirmed that the chitosan-POM nanoparticles were highly effective in TNAP inhibition (Figure 7). The most potent formulation was CS-TiW<sub>11</sub>Co nanoparticles with  $IC_{50} = 102.0 \pm 9.68$  nM.

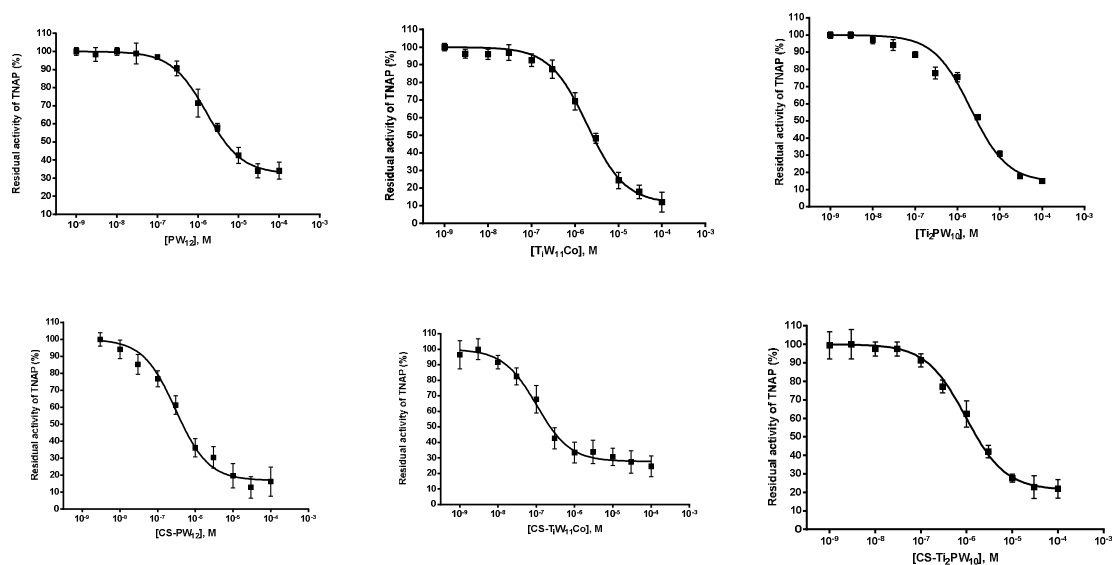


**Figure 7.** The graphs represent the  $IC_{50}$  values for unbound POMs and chitosan-POM nanoparticles when tested against tissue non-specific alkaline phosphatase (TNAP)

### Antiproliferation assay

#### Sulforhodamine B dye assay

The anticancer activities of the studied POMs were tested by a sensitive colorimetric assay, which uses sulforhodamine B dye for the determination of protein content in cancer cells. The unbound POMs and chitosan-POM nanoparticles were tested on HeLa cells and the  $IC_{50}$  value for each compound was determined. The results confirmed that the unbound POMs  $\{PW_{12}\}$ ,  $\{TiW_{11}Co\}$ , and  $\{Ti_2PW_{10}\}$  showed less inhibition towards HeLa cells with  $IC_{50}$  values of  $18.5 \pm 4.72$ ,  $9.21 \pm 2.64$ , and  $16.0 \pm 2.85$   $\mu M$ , compared to the chitosan-coated POMs CS- $PW_{12}$ , CS- $TiW_{11}Co$ , and CS- $Ti_2PW_{10}$  with  $IC_{50}$  values of  $8.37 \pm 1.84$ ,  $1.06 \pm 0.09$ , and  $5.36 \pm 1.57$   $\mu M$ , respectively. Amongst the tested compounds CS- $TiW_{11}Co_{40}$  showed the highest inhibition of HeLa cells, which was then taken for further studies.

**Table 3.** Alkaline phosphatase and anticancer activities of POMs and CS-POM nanoparticles

Code	Activity at TNAP (nM) (IC <sub>50</sub> ± SEM)	Anticancer activity on HeLa cells (μM) (IC <sub>50</sub> ± SEM)	Anticancer activity on Vero cells 10 (μM) (%Inhibition ± SEM)
{PW <sub>12</sub> }	1622 ± 22	18.5 ± 4.72	18 ± 2
CS-PW <sub>12</sub>	820.5 ± 31.4	8.37 ± 1.84	15 ± 3
{TiW <sub>11</sub> Co}	736.2 ± 12.7	9.21 ± 2.64	11 ± 4
CS-TiW <sub>11</sub> Co	102.0 ± 9.68	1.06 ± 0.09	9 ± 3
{Ti <sub>2</sub> PW <sub>10</sub> }	1050 ± 15	16.0 ± 2.85	14 ± 2
CS-Ti <sub>2</sub> PW <sub>10</sub>	301.7 ± 18.6	5.36 ± 1.57	13 ± 2
Levamisole	1375 ± 29		
Cisplatin		17.6 ± 5.94	17 ± 5

### Morphological evaluation of apoptosis by DAPI staining

The chitosan-POM nanoparticle CS-TiW<sub>11</sub>Co, which showed the lowest IC<sub>50</sub> (1.06 ± 0.096 μM), was selected to observe apoptosis with fluorescence microscopy. After staining with DAPI apoptotic bodies with condensed chromatin were observed when HeLa cells were treated with the selected compound. This observation confirmed that CS-TiW<sub>11</sub>Co nanoparticles kill HeLa cells by apoptosis.

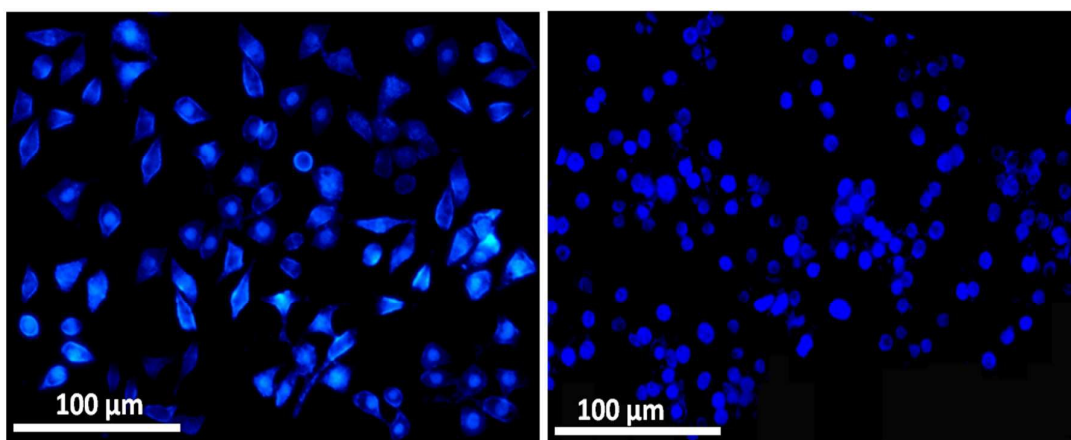


**Figure 8.** Morphological evaluation of untreated (left) and treated (right) HeLa cells with CS-TiW<sub>11</sub>Co nanoparticles. The fluorescence microscope (Nikon Eclipse-Ni Japan) was used to get images at an excitation and emission wavelengths of 358 and 461 nm, respectively

### Determination of reactive oxygen species (ROS)

The initiation of the production of ROS within HeLa cells by CS-TiW<sub>11</sub>Co was studied by using dichlorofluorescein diacetate (H<sub>2</sub>DCF-DA) dye and observed by fluorescence microscopy. Figure 9 shows that CS-TiW<sub>11</sub>Co nanoparticle-treated HeLa cells exhibit disintegrated cell membranes and condensed cellular protein (DNA) that may be due to oxidation of lipids and proteins.<sup>34</sup>

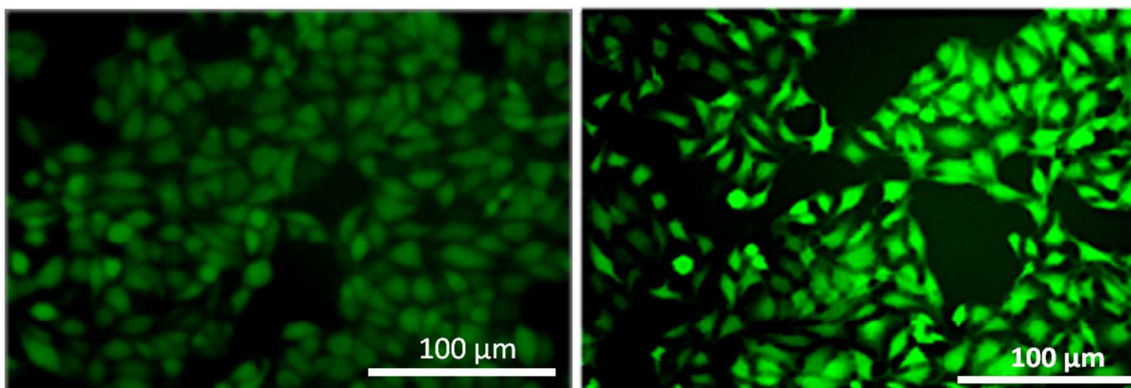


**Figure 9.** HeLa cells show the production of reactive oxygen species (ROS) when treated with CS-TiW<sub>11</sub>Co nanoparticles (right) and the ruptured cell membrane can be easily compared with untreated (left) HeLa cells. The image were captured at an excitation and emission wavelengths of 485 and 530 nm, respectively by using fluorescence microscope (Nikon Eclipse-Ni Japan)

### Conclusions

In the present study cobalt- and titanium-containing heteropolytungstates of the Keggin-type and their chitosan nanoparticles were synthesized by the ionotropic gelation technique. The unbound POMs and chitosan-POM nanoparticles were characterized and then investigated for anticancer and tissue non-specific alkaline phosphatase (TNAP) inhibition activities. All tested compounds were active against TNAP and HeLa cells, and CS-TiW<sub>11</sub>Co showed the highest inhibition for TNAP ( $IC_{50} = 102.0 \pm 9.68$  nM), and also anticancer activity ( $IC_{50} = 1.06 \pm 0.09$   $\mu$ M), and was the least toxic towards Vero normal cells ( $9 \pm 3$  %). Furthermore,

the apoptosis and ROS production by CS-TiW<sub>11</sub>Co was observed by fluorescence microscopy. Our work has demonstrated that CS-TiW<sub>11</sub>Co nanoparticles can serve as a potential drug for the treatment of cancer and bone metastasis.

### Materials and methods

Chitosan (YC-100) (M ~ 10,000 g/mol), Tissue non-specific alkaline phosphatase enzyme (TNAP), Levamisole, Tris-HCl, Tris base, MgCl<sub>2</sub>, ZnCl<sub>2</sub>, DMEM High glucose, Fetal bovine serum (FBS), Penicillin, streptomycin and lysozyme of chicken egg white were purchased from Sigma-Aldrich, Steinheim, Germany. were purchased from Sigma-Aldrich, Steinheim, Germany. The Human cervical adenocarcinoma (HeLa) cell line and African green monkey kidney (Vero) cell line were purchased from American Type Culture Collection (ATCC), USA.

### Experimental

#### Synthesis of POMs

The selected POM salts Na<sub>3</sub>[PW<sub>12</sub>O<sub>40</sub>]·6H<sub>2</sub>O {PW<sub>12</sub>}, K<sub>4</sub>H<sub>3</sub>[Ti<sub>2</sub>PW<sub>10</sub>O<sub>40</sub>]·35H<sub>2</sub>O {Ti<sub>2</sub>PW<sub>10</sub>} and K<sub>6</sub>H[TiW<sub>11</sub>CoO<sub>40</sub>]·H<sub>2</sub>O {TiW<sub>11</sub>Co} (Figure 1) were synthesized according to the published procedures and characterized by FT-IR (Figure 3).<sup>35-37</sup> Furthermore, polyanions [PW<sub>12</sub>O<sub>40</sub>]<sup>3-</sup> and [Ti<sub>2</sub>PW<sub>10</sub>O<sub>40</sub>]<sup>7-</sup> were characterized by <sup>31</sup>P-NMR (Figure 2).

#### Synthesis of Chitosan-PW<sub>12</sub> (CS-PW<sub>12</sub>)

CS-PW<sub>12</sub> nanoparticles were synthesized by stirring 0.50 g (0.71 mM) of CTS in 70 mL distilled water for 5 min. The resultant solution was then filtered (solution A). Similarly, 1.83 g (0.6 mM) of {PW<sub>12</sub>} was dissolved in 30 mL distilled water (solution B). Solution B was then added dropwise to solution A, forming a gel-like precipitate which was separated by filtration and washed several times with water and then air-dried. The obtained product was characterized by FTIR (see Figure 3).

### **Synthesis of Chitosan-[Ti<sub>2</sub>PW<sub>10</sub>O<sub>40</sub>] (CS-Ti<sub>2</sub>PW<sub>10</sub>)**

CS-Ti<sub>2</sub>PW<sub>10</sub> nanoparticles were synthesized under the same conditions as CTS-PW<sub>12</sub>. However, solution B was prepared by dissolving 1.00 g (0.34 mM) of Ti<sub>2</sub>PW<sub>10</sub> in distilled water. The obtained product was characterized by FTIR (see Figure 3).

### **Synthesis of Chitosan-[TiW<sub>11</sub>CoO<sub>40</sub>] (CS-TiW<sub>11</sub>Co)**

CS-TiW<sub>11</sub>Co nanoparticles were synthesized under the same conditions as CTS-PW<sub>12</sub>. However, solution B was prepared by dissolving 1.11g (0.34 mM) of {TiW<sub>11</sub>Co} in distilled water. The obtained product was characterized by FTIR (see Figure 3).

### **Characterization of nanoparticles**

The nanoparticles were characterized by investigation of particle size, zeta potential and surface morphology. Dynamic light scattering and electrophoretic light scattering techniques were used to determine the particle size distribution and zeta potential of the nanoparticles. Scanning electron microscopy (SEM) was used to observe the surface morphology of the nanoparticles. Fourier transform infrared (FTIR) spectroscopy was used to identify the vibrational bands.

### **Determination of entrapment efficiency**

A previously described method with a slight modification was used to determine the entrapment efficiency of the CS-POM nanoparticles.<sup>14</sup> Briefly, a predetermined weight of nanoparticles was centrifuged at 12,000 rpm for 40 min and the supernatant was investigated by UV-visible spectroscopy to determine the amount of non-entrapped POM in the formulation.

$$\text{Entrapment efficiency (\%)} = \left( \frac{\text{Total POM in formulation} - \text{Free POM}}{\text{Total POM in formulation}} \right) \times 100$$

### ***In vitro* dissolution studies**

To determine the release mechanism of the POMs from the nanoparticles, *in vitro* dissolution studies were carried out by following a previously reported method.<sup>14</sup> The nanoparticles were centrifuged at 12,000 rpm for 40 min and the pellet obtained was redispersed in 900 mL phosphate buffered saline (PBS) at pH 7.4. A small amount of lysozyme (1.2 µg/mL) was also added to promote chitosan degradation in PBS. The experiment was conducted on a magnetic stirrer with 75 rpm at 37 °C. Samples were taken at pre-determined time intervals and the amount of POM released in the medium was calculated by using a standardized curve. The release kinetics (zero order and first order) and release mechanism (Higuchi and Peppas models) were determined by following mathematical equations:

$$\text{Zero order rate equation} \quad Q_t = Q_o K_o t \quad (1)$$

$Q_o$  and  $Q_t$  represent the amount of drug release at ( $t_o$ ) and at a specified time ( $t$ ) whereas  $k_o$  is the zero order rate constant.

$$\text{First order rate equation} \quad \ln M = -k_1 t + \ln M_o \quad (2)$$

$M_o$  is the initial amount of POM and  $M_t$  is the remaining amount of POM at time  $t$  and  $k_1$  is the first order rate constant.

$$\text{Higuchi equation} \quad M = k_H t^{1/2} \quad (3)$$

$M$  is the amount of POM released at time  $t$  and  $K_H$  is the Higuchi rate equation

$$\text{Peppas model} \quad \ln (M_t/M_\infty) = \ln k_p + n \ln t \quad (4)$$

$(M_t/M_\infty)$  is the fraction of drug released at time  $t$  and  $n$  is the slope which determines the type of diffusion from the polymer matrix.

### **Enzyme inhibition studies against TNAP**

Enzyme inhibition studies were carried out by following a previously reported spectrophotometric method.<sup>38</sup> Briefly, TNAP was diluted in an assay buffer (pH 9.5) comprised of Tris-HCl (50 mM), MgCl<sub>2</sub> (5 mM), ZnCl<sub>2</sub> (0.1 mM), and glycerol (50%). The

enzyme substrate *p*-nitrophenyl phosphate (*p*-NPP) was dissolved in the same buffer without glycerol. The experiment was started by mixing enzyme (10  $\mu$ L) with test compound (10  $\mu$ L) and kept at 37 °C for 10 min (pre-incubation). The enzyme substrate (*p*-NPP) was added and again incubated for 30 min. A yellow coloured product (*p*-nitrophenolate) was formed and the absorbance was measured at 405 nm using an ELISA plate reader (Bio-TekELx 800™, Instruments, Inc. USA). Each experiment was performed in triplicate and the results obtained were presented as IC<sub>50</sub> values calculated by using Prism 5.0 (GraphPad Software, San Diego, CA, USA).

### **Cell lines and cell cultures**

HeLa cells were cultured and maintained in DMEM High glucose medium supplemented with L-glutamine (2.0 mM), penicillin (100 U/mL) and streptomycin (100  $\mu$ g/mL) and FBS (10%). The culture flasks were kept in a specialized incubator providing CO<sub>2</sub> (5%) at a constant temperature of 37 °C. To conduct the antiproliferation assay, the HeLa cells were seeded in 96-well plates with a density of 20,000 cells per well.

### **Antiproliferation assay**

A common, highly sensitive colorimetric assay utilizing sulphorhodamine B dye, which binds with cellular proteins, was used to determine the degree of cytotoxicity.<sup>39</sup> HeLa cells were harvested in 96-well plates and treated with different concentrations of the test compounds for 24 h. The plates were removed from the incubator and treated with ice-cold TCA (50 %) and kept at 4 °C. The plates were gently rinsed with PBS and then treated with sulforhodamine B dye (0.4 %) and kept again for 30 min at room temperature. In order to remove unbound dye the plates were treated with 1 % acetic acid solution. The cell-bound dye was solubilized by adding Tris base (10 mM) and left for some time at room temperature. The absorbance was measured at 490 nm subtracting the background measurement at 630 nm.

### **Evaluation of apoptosis by fluorescence microscopy**

#### **Morphological evaluation of apoptosis with DAPI staining**

HeLa cells ( $1.4 \times 10^4$ ) were cultured in a 2-well sterile chamber slide, treated with the test compounds and incubated for 24 h. Formalin (4%) was used for cell fixation. After washing with PBS the cells were stained with DAPI (10  $\mu\text{g/mL}$ ) for 10 min. in the dark and examined under a fluorescence microscope (Nikon Eclipse-Ni Japan) with excitation and emission wavelengths of 358 and 461 nm, respectively.<sup>40</sup>

#### **Determination of intracellular reactive oxygen species (ROS) production**

The morphological evaluation of ROS production in treated HeLa cells was observed in order to determine characteristic changes in the cell membrane and condensed nuclei, due to the oxidation of lipids and proteins. HeLa cells ( $1.2 \times 10^6$ ) were treated with the test compounds for 24 h and then fixed with formalin (4%) and stained with DCFH-DA. After 10 min. of incubation at room temperature, the slide was studied under a fluorescence microscope with excitation and emission wavelengths of 485 and 530 nm, respectively.<sup>41</sup>

#### **Acknowledgements**

U. K. thanks Jacobs University and the German Science Foundation (DFG) for research support over the years. A. H. thanks Deutscher Akademischer Austauschdienst (DAAD) for a Ph.D. fellowship. S.A.J. acknowledges Department of Science and Technology (DST), Government of India (GoI) for sanctioning leave to carry out research in Jacobs University, Bremen, Germany. J.I. is thankful to the Organization for the Prohibition of Chemical Weapons (OPCW), The Hague, The Netherlands and the Higher Education Commission of Pakistan for the financial support through Project No. 20-3733/NRPU/R&D/14/520.

## References

1. U. Kortz, A. Mueller, J. van Slageren, J. Schnack, N. S. Dalal and M. Dressel, *Coord. Chem. Rev.*, 2009, **253**, 2315-2327.
2. M. T. Pope and A. Müller, *Angew. Chem., Int. Ed.*, 1991, **30**, 34-48.
3. N. V. Izarova, M. T. Pope and U. Kortz, *Angew. Chem., Int. Ed.*, 2012, **51**, 9492-9510.
4. M. T. Pope and U. Kortz, *Encyclopedia of Inorganic and Bioinorganic Chemistry*, 2012.
5. T. Yamase and M. Pope, *Polyoxometalate chemistry for nano-composite design*, Springer Science & Business Media, 2006.
6. J. T. Rhule, C. L. Hill, D. A. Judd and R. F. Schinazi, *Chem. Rev.*, 1998, **98**, 327-358.
7. A. Ogata, H. Yanagie, E. Ishikawa, Y. Morishita, S. Mitsui, A. Yamashita, K. Hasumi, S. Takamoto, T. Yamase and M. Eriguchi, *Br. J. Cancer*, 2008, **98**, 399-409.
8. H. Thomadaki, A. Karaliota, C. Litos and A. Scorilas, *J. Med. Chem.*, 2007, **50**, 1316-1321.
9. Z. Dong, R. Tan, J. Cao, Y. Yang, C. Kong, J. Du, S. Zhu, Y. Zhang, J. Lu and B. Huang, *Eur. J. Med. Chem.*, 2011, **46**, 2477-2484.
10. L. Wang, K. Yu, B. B. Zhou, Z. H. Su, S. Gao, L. L. Chu and J. R. Liu, *Dalton Trans.*, 2014, **43**, 6070-6078.
11. F. Zhai, X. Wang, D. Li, H. Zhang, R. Li and L. Song, *Biomed. Pharmacother.*, 2009, **63**, 51-55.
12. L. Wang, B. B. Zhou, K. Yu, Z. H. Su, S. Gao, L. L. Chu, J. R. Liu and G. Y. Yang, *Inorg. Chem.*, 2013, **52**, 5119-5127.
13. H. U. Gerth, A. Rompel, B. Krebs, J. Boos and C. Lanvers-Kaminsky, *Anti-cancer drugs*, 2005, **16**, 101-106.
14. D. Menon, R. T. Thomas, S. Narayanan, S. Maya, R. Jayakumar, F. Hussain, V.-K. Lakshmanan and S. Nair, *Carbohydr. Polym.*, 2011, **84**, 887-893.
15. I. León, V. Porro, S. Astrada, M. Egusquiza, C. Cabello, M. Bollati-Fogolin and S. Etcheverry, *Chemico-biolo. Interact.*, 2014, **222**, 87-96.
16. H. Yanagie, A. Ogata, S. Mitsui, T. Hisa, T. Yamase and M. Eriguchi, *Biomed. Pharmacother.*, 2006, **60**, 349-352.
17. T. Yamase, *J. Mater. Chem.*, 2005, **15**, 4773-4782.
18. G. R. Mundy, *Nat. Rev. Cancer*, 2002, **2**, 584-593.
19. G. D. Roodman, *New Engl. J. Med.*, 2004, **350**, 1655-1664.
20. J. L. Millán, *Mammalian alkaline phosphatases: from biology to applications in medicine and biotechnology*, John Wiley & Sons, 2006.
21. R. Raza, A. Matin, S. Sarwar, M. Barsukova-Stuckart, M. Ibrahim, U. Kortz and J. Iqbal, *Dalton Trans.*, 2012, **41**, 14329-14336.
22. S.-Y. Lee, A. Fiene, W. Li, T. Hanck, K. A. Brylev, V. E. Fedorov, J. Lecka, A. Haider, H.-J. Pietzsch and H. Zimmermann, *Biochem. Pharmacol.*, 2015, **93**, 171-181.

23. L. Zhang, J. M. Chan, F. X. Gu, J.-W. Rhee, A. Z. Wang, A. F. Radovic-Moreno, F. Alexis, R. Langer and O. C. Farokhzad, *ACS nano*, 2008, **2**, 1696-1702.
24. K. A. Whitehead, R. Langer and D. G. Anderson, *Nature reviews Drug discovery*, 2009, **8**, 129-138.
25. N. Bertrand and J.-C. Leroux, *J. Controlled Release*, 2012, **161**, 152-163.
26. V. M. Pandya, U. Kortz and S. A. Joshi, *Dalton Trans.*, 2015, **44**, 58-61.
27. H. S. Shah, R. Al-Oweini, A. Haider, U. Kortz and J. Iqbal, *Toxicol. Rep.*, 2014, **1**, 341-352.
28. E. Markovsky, H. Baabur-Cohen, A. Eldar-Boock, L. Omer, G. Tiram, S. Ferber, P. Ofek, D. Polyak, A. Scomparin and R. Satchi-Fainaro, *J. Controlled Release*, 2012, **161**, 446-460.
29. S. M. Moghimi, A. C. Hunter and J. C. Murray, *Pharmacol. Rev.*, 2001, **53**, 283-318.
30. M. R. Kumar, R. A. Muzzarelli, C. Muzzarelli, H. Sashiwa and A. Domb, *Chem. Rev.*, 2004, **104**, 6017-6084.
31. M. Rinaudo, *Prog. Polym. Sci.*, 2006, **31**, 603-632.
32. G. Hungerford, F. Hussain, G. R. Patzke and M. Green, *Phys. Chem. Chem. Phys.*, 2010, **12**, 7266-7275.
33. A. Anitha, V. D. Rani, R. Krishna, V. Sreeja, N. Selvamurugan, S. Nair, H. Tamura and R. Jayakumar, *Carbohydr. Polym.*, 2009, **78**, 672-677.
34. R. P. Rastogi, S. P. Singh, D.-P. Häder and R. P. Sinha, *Biochem. Biophys. Res. Commun.*, 2010, **397**, 603-607.
35. N. Chen and R. Yang, *J. Catal.*, 1995, **157**, 76-86.
36. W. Kraus, H. Stephan, A. Röllich and G. Reck, *Acta Crystallogr. Sect. E: Struct. Rep. Online*, 2005, **61**, 35-37.
37. P. Domaille and W. Knoth, *Inorg. Chem.*, 1983, **22**, 818-822.
38. J. Iqbal, *Anal. Biochem.*, 2011, **414**, 226-231.
39. P. Skehan, R. Storeng, D. Scudiero, A. Monks, J. McMahon, D. Vistica, J. T. Warren, H. Bokesch, S. Kenney and M. R. Boyd, *J. Natl. Cancer Inst.*, 1990, **82**, 1107-1112.
40. R. V. Priyadarsini, R. S. Murugan, S. Maitreyi, K. Ramalingam, D. Karunakaran and S. Nagini, *Eur. J. Pharmacol.*, 2010, **649**, 84-91.
41. S. Dhandayuthapani, P. Marimuthu, V. Hörmann, J. Kumi-Diaka and A. Rathinavelu, *J. Med. Food*, 2013, **16**, 139-146.